A Parametric Analysis of the Aerodynamic Characteristics of Volleyballs in Turbulent Flow

Hans J. Thomas

A thesis

submitted in partial fulfillment of the

requirements for the degree of

Master of Science in Aeronautics and Astronautics

University of Washington

2012

Robert Breidenthal, Chair

James Riley

Program Authorized to Offer Degree:

Aeronautics and Astronautics

University of Washington

Abstract

A Parametric Analysis of the Aerodynamic Characteristics of Volleyballs in Turbulent Flow

Hans J. Thomas

Chair of Supervisory Committee:
Professor Robert E. Breidenthal
Aeronautics and Astronautics

A wind tunnel experiment was conducted to compare the flight path characteristics and drag of current models of volleyballs. An open circuit low speed wind tunnel was primarily used to gather lift and drag data on multiple models of volleyballs in super-critical Reynolds number flows. The models tested were the Baden VX5E-01, Baden VX450C-230, Baden VX450-02, Mikasa MVA200, and Molten V5M5000. Analysis was conducted to determine the relationship between cavity dimensions on the balls and the lift and drag characteristics of the balls. Conditions were based on indoor volleyball conditions set by the International Federation of Volleyball (FIVB) with Reynolds numbers ranging from $2x10^5$ to $4.3x10^5$. Recommendations were provided for future designs of volleyballs to improve aerodynamic performance.

TABLE OF CONTENTS

LIST OF FIGURES

LIST OF TABLES

NOMENCLATURE

D	Ball diameter
R	Specific gas constant for air
S	Ball frontal area
P_{atm}	Atmospheric pressure
T	Temperature
q	Dynamic pressure
μ	Dynamic viscosity of air
ρ	Density of air
V	Uniform Airflow Velocity
Re	Reynolds number
L	Lift
Y	Side Force
L_{tot}	Total Lift
θ	Total Lift Angle
c_l	Coefficient of lift
c_y	Coefficient of side force
C_L	Coefficient of total lift
C_D	Coefficient of drag
C	Cross sectional area of tunnel
ε_s	Solid blockage factor
ε_w	Wake blockage factor
ε	Total blockage factor
T_0	Standard day temperature
P_0	Standard day atmospheric pressure
μ_0	Standard day dynamic viscosity
ρ_0	Standard day density
θ*	Momentum thickness
SA	Surface area
d	Cavity depth
b	Cavity width
z	Cavity factor 1
y	Cavity factor 2

ACKNOWLEDGEMENTS

The initial desire to look into the performance characteristics of volleyballs came from Baden Sports Inc. out of Federal Way, WA. Although they did not fund the research in that they did not pay for the man-hours or the use of the wind tunnels, they did supply all of the volleyballs tested and provided funding for the apparatus used to mount the balls to the balance. I would like to thank them for their assistance in this research and for being patient with the results.

The implementation of this experiment could not have been completed without the assistance of Robert Gordon and Nathan Precup. Both were instrumental in constructing the apparatus to hold the balls, calibrating the balance, and troubleshooting the data processing. I would also like to thank the University of Washington Aeronautical Laboratory for allowing me to use the Kirsten Wind Tunnel on short notice.

I would like to thank Professor Robert Breidenthal who brought this project to my attention and guided me while I searched for meaning in the data. And of course, to my wife, Noelle, who put up with my long absences while running experiments and patiently supported me through all my procrastination in writing this thesis.

CHAPTER 1: INTRODUCTION

Volleyball was invented in 1895 by William G. Morgan at the Holyoke, MA YMCA as a less intense alternative to basketball. Its popularity grew over the years and expanded beyond the borders of the United States. It is now played in over 150 nations and is one of the most popular sports in the world.

The regulations for volleyballs (as with most sports balls) are quite restrictive and are set by the Federation Internationale de Volleyball (FIVB). The rules dictate the material, shape, weight, size, pressure, and even color scheme allowed on competition volleyballs (Thorsteinsson). However, they have remained quite lax when it comes to the surface pattern of the balls, requiring only that the ball have a range of 8-18 panels. Yet for almost a hundred years, the design of the volleyball has not changed. Manufacturers have used the traditional design of the ball with 18 panels that most people are familiar with.

However in 2008, Mikasa Sports USA (Irvine, CA) unveiled a radical new design for a volleyball that had only eight panels and had small dimples on the surface, similar to a golf ball. In their press release, Mikasa Sports USA claimed that the new design gave the ball a truer flight path and greater ball-control (Mikasa Sports, 2008). Soon after, the Molten Corporation (Hiroshima, Japan) developed a new design for a volleyball that used their patented FLISTATEC® (Flight Stability Technology) which consists of raised hexagons on the surface that Molten claims reduces the drag and improves the stability of the ball. Molten also modified the panel design for the ball, though they claimed this was more for aesthetics than aerodynamics (Molten Corporation). Finally, Baden developed their own advanced ball that utilized the same pattern as their traditional balls but added dimples.

The aerodynamic characteristics of a volleyball in flight are quite complex. Trying to understand the flight characteristics of a simple sphere in turbulent flow is difficult enough, however with volleyballs the seams add irregularities to the surface. Combining this with the fact that the ball can be launched in any orientation and later rotate to other orientations leads to a truly complex system.

Previous experiments have been conducted to study the aerodynamic characteristics of volleyballs. In 1988, a group from Peking University looked at wake vortices produced by non-spinning volleyballs in a wind tunnel to try and understand the unpredictable path taken by a floater (non-spinning) serve (Wei, Lin, & Liu, 1988). In 2010, Molten commissioned research using an impact-type ball ejection device to measure the accuracy of different volleyball models in non-spinning flight (Asai, Ito, Seo, & Hitotsubashi, 2010). The difference between research described in this paper and previous

experiments is that this research aimed to look at multiple models with large and small changes to the model orientation to better understand how model design and orientation affect the aerodynamic characteristics of a non-spinning volleyball in flight.

This research sought to compare and contrast the flight path stability and drag characteristics of different non-spinning volleyballs in different orientations. For the purposes of this research, flight path stability will be measured by using lift values, with the ideal flight path stability design being one that produces no lift and therefore does not deviate from its initial trajectory. The ideal volleyball should also produce a low amount of drag, however the flight path stability characteristic is considered by manufacturers to be more important. By identifying the performance characteristics of different designs and noting the significant differences in the designs, it was hoped that a relationship could be established between certain design characteristics and corresponding performance characteristics. This would then aid future design of high performance sports balls.

CHAPTER 2: EXPERIMENTAL PROCEDURE

2.1 Constraints

The major constraint of this experiment was that the ball could not spin. This was done for two reasons, the first being that to have adapted the system to spin would have required mounting the ball with the spar perpendicular to the airflow. This would have added more drag to the system, disrupted the flow, and provided less accurate data than having the sting behind the ball in the flow. The second reason is that a spinning ball is more stable than a non-spinning ball. In fact, the float serve is used because it causes the ball to act unpredictably and follow an unstable trajectory, similar to the knuckleball in baseball. By not having the ball spin, the characteristics of the balls could be observed in their least-aerodynamically-sound configuration.

Wind speed was also a constraint. The Low Speed Wind Tunnel (also known as the 3x3 Tunnel) has a fan that pulls air through the wind tunnel. The fan's rate of rotation remains constant while the pitch of the fan blades is altered to change the dynamic pressure in the tunnel. At low speeds, the blades cause the air in the tunnel to circulate, which would skew the data. For this reason, data was not taken below 41 feet per second (fps). At high speeds, the ball became more unstable and began to oscillate on the balance, so the limit for maximum speed set at around 130 fps. Observations have been made that men hit a floater serve at 44.5-54 fps, so the testing from this research is applicable to men's volleyball (Hayrinen, Lahtinen, Mikkola, Honkanen, Paananen, & Blomqvist, 2007).

Due to time and resource constraints, not every possible orientation of each model was studied. Instead three very different configurations for each model were chosen and were then altered by +/- 10 degrees. This provided a full concept of the possible characteristics of each model, but by no means a complete one.

2.2 Wind Tunnel Testing

Most of the experiments for this project were done in the Low Speed Wind Tunnel at the University of Washington, Seattle, WA. The tunnel allowed for adequate flow rates and minimal obstruction of airflow. It is an open-circuit wind tunnel with a three foot by three foot test section. Static probes were placed forward and aft of the test section to determine the dynamic pressure in the test section as well as the ambient pressure. A temperature probe was also inserted to gather the ambient temperature. A sting mount was lowered into the test section from above and attached to the balance. The balance was a 0.75 Mark XIII cylindrical balance built by the Task Corporation (the design was later

purchased by Able Corporation which was then purchased by Aerophysics Research Instruments, LLC). It is a six component strain gage balance rated to 200 lbs. lift or side force, 50 lbs. of drag, and 20 inch-lbs. of roll moment (the roll elements on this balance were broken, however since roll moment was not necessary to the research, it did not hinder operations).

Additional testing was performed on a limited number of models and orientations using the Kirsten Wind Tunnel at the University of Washington Aeronautical Laboratory. The Kirsten Wind Tunnel is a closed circuit wind tunnel with a test section that is eight feet high, twelve feet wide and ten feet long. The Low Speed Tunnel cannot obtain accurate enough data at speeds below the critical Reynolds number (the Reynolds number for an object at which a turbulent boundary layer is formed so that boundary layer separation is delayed and drag is often reduced. This is also known as the drag crisis) so the Kirsten Tunnel was used to see when the ball reached the critical Reynolds number and how the balls performed at speeds below it.

For every model being tested, three unique configurations were chosen. These configurations were chosen such that if a photo was taken of the configuration upwind, it would be different from any other configuration of that model. A three inch plaster mold with bolts was epoxied to every ball tested. The mold was then secured with four screws to an aluminum mount which allowed the ball to pitch up and down by five degrees. The mount was curved so that as the ball was rotated, the center of the ball remained in the centerline of the balance. The complete apparatus used in the trials is shown in Figure 1.

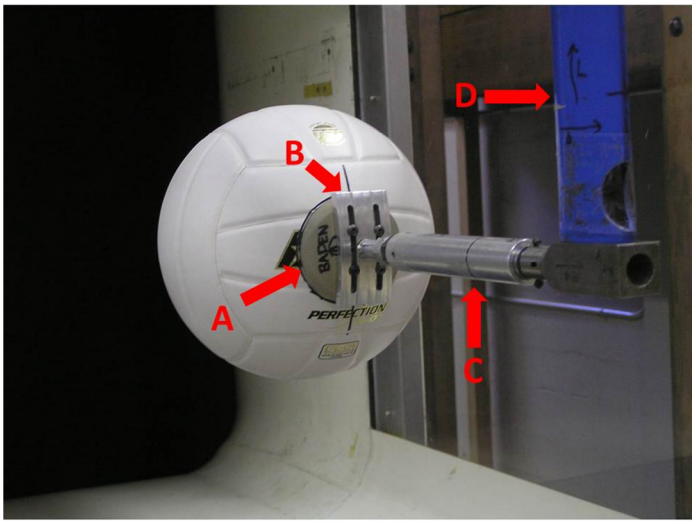

Figure 1: Testing Apparatus. The grey disk is the mold (A) that was epoxied to each ball. Attached to it is the mount (B) that allows for adjustment of orientation. The smooth grey cylinder is the balance (C). It is screwed into the spar (D) that extends down from the roof of the tunnel.

The electrical signals from the sensors in the balance as well as the pressure and temperature signals were transmitted to a Labview program. This removed the offset data and converted the electrical signals to usable data (forces, moments, pressures, and temperatures) based on the conversion rates determined during calibration. The program also accounted for force interactions and took time averages of the data. The offset values were taken with the ball on the mount and the tunnel fan turned off. The fan was then turned on and the tunnel brought up to a dynamic pressure of 20.00 pounds per square feet (psf). Data was acquired as 10 second time averages once the dynamic pressure had stabilized to a steady state condition. The dynamic pressure was then reduced in increments of 0.50 +/-0.05 psf and 10 second time averages of the data were again taken representing one data point of the run. This was repeated all the way down to 2.00 psf. All of that data represented one run of one orientation. Each configuration was run with the mount set so that the mold was centered in the mount (0 degree pitch), was lowered in the mount (+5 degree pitch), and was raised in the mount (-5 degree pitch). This created three orientations for each configuration, resulting in 9 total runs and orientations for each model. An image of each configuration can be found in Appendix C.

2.3 Data Processing

Once the runs were complete, the data was converted to a Microsoft Excel file and imported into a MATLAB code written for this experiment (see Appendix B). It was important to get non-dimensionalized characteristics that were independent of ambient temperature and pressure. The data was collected over many months, creating a wide variety of environmental conditions. Also, after a few runs in the Low Speed Tunnel, the ambient temperature increased by as much as 5° C.

The code received inputs of forces, pitch and yaw moments, dynamic pressure, atmospheric pressure, and ambient temperature. The first step was to nondimensionalize the uniform velocity at each data point. To do this, atmospheric pressure and temperature were converted to psf and degrees Rankine, respectively. The instantaneous dynamic viscosity of air was derived using Sutherland's Law (Wilcox, 2010) in equation (1) and the density was derived from the ideal gas law in equation (2).

$$\mu = 2.27 \times 10^{-8} \frac{slug}{ft \cdot s \cdot R^{0.5}} \times \frac{T^{1.5}}{T + 198.6°R} \quad (1)$$

$$\rho = {P_{atm}}/{RT} \quad (2)$$

The velocity at each data point was determined using the relationship:

$$V_U = \sqrt{2q/\rho} \quad (3)$$

This allowed the Reynolds number of the flow to be calculated as

$$Re_U = V_U \rho d/\mu \quad (4)$$

The next step was to nondimensionalize the forces. This was done with a frontal area of:

$$S = \frac{\pi}{4}(d)^2 \quad (5)$$

The forces data gathered from the wind tunnels labeled lift as the force perpendicular to the earth's surface and side force as the force parallel to the earth's surface but perpendicular to the airflow. Total lift, being the magnitude of the lift and side force (see Figure 2), was determined because it is more relevant to practical application of volleyball. The experiment is looking for the most amount of lift that could be created (worst case scenario) and taking a magnitude determines the max lift of that orientation without having to rotate the apparatus around the drag axis. The angle of total lift, θ, was obtained in order to determine how the direction of the total lift shifted as the velocity of the ball changed. It was calculated by taking the arctangent of the lift over the side force. The force coefficients were calculated using:

$$c_{l_U} = {}^{L}/_{qS} \quad (6)$$

$$c_{y_U} = {}^{Y}/_{qS} \quad (7)$$

$$C_{L_U} = {}^{L_{tot}}/_{qS} \quad (8)$$

$$C_{D_U} = {}^{D}/_{qS} \quad (9)$$

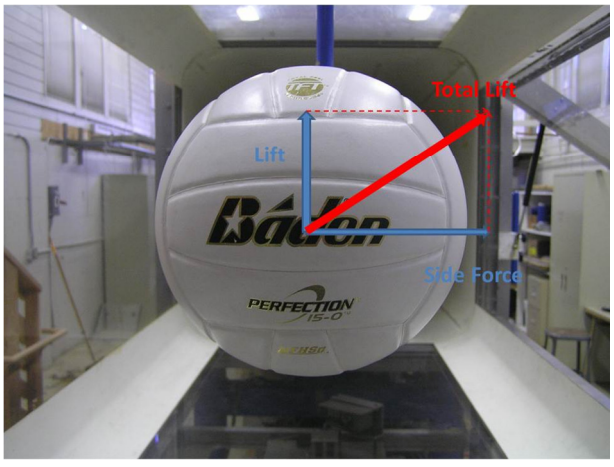

Figure 2: Diagram of Total Lift

These values however do not account for blockage due to the ball and wake behind the ball impeding the flow and decreasing the dynamic pressure. Blockage correction factors were calculated and applied using equations found in Pankhurst's **WIND-TUNNEL TECHNIQUE** (Pankhurst & Holder, 1965).

$$\varepsilon_s = 0.809\left(S/C\right)^{1.5} \quad (10)$$

$$\varepsilon_w = \frac{1}{4}\left(S/C\right)C_{D_U} \quad (11)$$

$$\varepsilon = \varepsilon_s + \varepsilon_w \quad (12)$$

$$V = V_U(1 + \varepsilon) \quad (13)$$

$$Re = Re_U(1 + \varepsilon) \quad (14)$$

$$C_L = C_{L_U}(1 - 2\varepsilon) \quad (15)$$

$$C_D = C_{D_U}(1 - 2\varepsilon) \quad (16)$$

Each runs performance, though nondimensionalized, could not be compared at each data point because the Reynolds numbers at each data point were not exactly the same. The dynamic pressure at a data point in one run could be as different as 0.1 psf when compared to a corresponding data point in another run. The temperature and ambient pressure were also different during different runs, resulting in different Reynolds numbers for corresponding data points. To make the runs comparable, a range for velocity was established from 44 to 100 fps. Reynolds numbers for these velocities were determined at standard day conditions (15℃ and 29.92 in Hg). Values for coefficients of lift and drag could then be extrapolated from each run through interpolation, allowing for mean and standard deviation data to be determined based on the populations of configurations and models.

2.4 Measurements

In order to quantify the differences in the ball designs, measurements were taken of the dimensions of the seams and the dimples using a Mitutoyo MN85 caliper with built-in depth gauge. The caliper is accurate to 0.001 inch. The depth gauge was filed to a point so that it could fit inside the seams of the balls. Seam dimensions were measured at eight different points at the ball then averaged to get the seam/dimple depth and width. Seam lengths were measured directly on the ball, while dimple surface

area was calculated by counting the amount of dimples in a three inch by three inch patch on the ball, multiplying that number by 23.8794 (based on the surface area of the ball being 214.9146 in^2), and multiplying by the surface area of each dimple.

CHAPTER 3: RESULTS

3.1 Evolution of a Volleyball

Due to the volleyball rules governing volleyball design, there are only three areas that can be changed in the design of a volleyball: seam design, material, and dimpling. In order to isolate how each of these areas affects a ball, three models by Baden were examined. These were the Baden VX5E-01 (Original), the VX450C-230 (Lexum), and the VX450-02 (Dimple). The Lexum differs mainly from the Original in that it is made from composite materials instead of leather (the seam dimensions are a little different in these balls as well, although the overall pattern is still the same.) This composite material is not as smooth as the leather material of the Baden Original ball. The Dimple differs from the Lexum in that it has dimples added to it. In this way each change to the design could be looked at to see how it affected the performance of the volleyball. These three models can be seen in Figure 3. Though the seam designs of these balls are the same, there is a small difference in the seam dimensions: the width and depth of the seams are not the same and are noted in Table 1. Images of their texture and their seams can be seen in Appendix D and Appendix E, respectively.

Figure 3: Baden Volleyballs. A front profile photo of configuration 1 for the Baden VX5E-01 Original (a), VX450C-230 Lexum (b), and VX450-02 Dimple (c).

Each ball was run nine different times, so plotting all of the runs on the same graph would be very busy and difficult to interpret. Figure 4 shows the lift and drag plots for Baden balls. The mean and standard deviation of each of the runs at each major configuration is shown with the mean axis on the left and the standard deviation axis on the right. This shows the general profile of balls as well as how a

change of 5 degrees in either direction will affect the profile. Mean plots have diamonds for markers; standard deviation plots have asterisks for markers.

Table 1: Seam Dimensions

Make	Model	Depth (in)	Width (in)	Aspect Ratio (width/depth)	Length (in)	Surface Area (in^2)
Baden	VX5E-01 (Original)	0.027	0.282	10.3	153.78	43.30
Baden	VX450C-230 (Lexum)	0.029	0.291	10.1	153.78	44.68
Baden	VX450-02 (Dimple)	0.027	0.297	10.9	153.78	45.72
Mikasa	MVA200	0.021	0.303	14.7	98.98	29.98
Molten	V5M5000	0.020	0.230	11.4	161.58	37.15
Baden	VX5E-01 (Min Skiv)	0.027	0.170	6.3	153.78	26.14
Baden	VX5E-01 (No Skiv)	0.007	0.135	19.8	153.78	20.74

The results would appear to show that switching to a composite material and adding dimples had little to no effect at reducing the drag and lift characteristics of the volleyball when compared to the original design. Generally the Lexum ball produced more lift and drag than the Original ball. When it did come close to matching the mean performance of the Original ball (start of Configuration 1), it did so with a higher standard deviation. The Dimple ball performed overall as well as the Original ball, though it was not clear what benefit the dimples provided over the original design. If the Dimple ball is viewed as a modification of the Lexum ball, it can be inferred that the dimples reverse the negative attributes of the Lexum ball, to the effect that they return the performance back to that of the Original ball.

It should also be noted that at high speeds, all balls approached a mean coefficient of drag of about 0.2 and as the speed increased, the means generally increased and the standard deviation of those mean values decreased. This shows that the ball's drag characteristics become more stable at high speeds and that orientation of the ball becomes less relevant. The standard deviation for the coefficient of lift was higher than that of drag and was consistent, neither increasing nor decreasing significantly over time. For the first and second configurations, the variation stayed between 0.02 and 0.04. Looking at all the configurations, there is no clear trend for the coefficient of lift either in mean or standard deviation, which would make it seem that the coefficients of lift at these speeds are independent of Reynolds number.

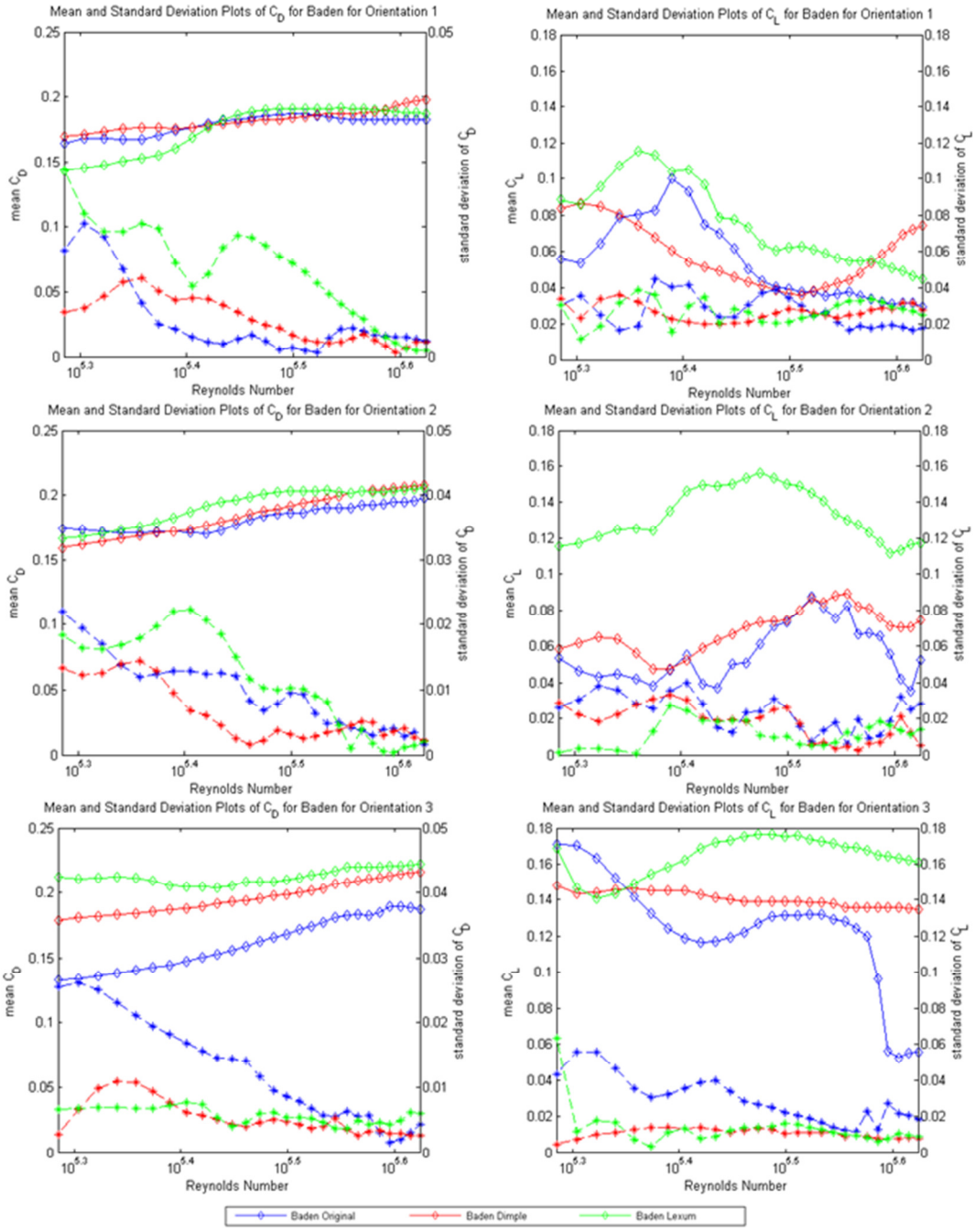

Figure 4: Baden Balls at Different Configurations. Mean values are indicated by diamonds and standard deviations are indicated by asterisks.

To understand the effects of the property changes further, some of the balls were taken to the Kirsten Wind Tunnel where the characteristics of the ball could be studied at lower speeds. Due to time constraints, only a few of the configurations could be tested in the Kirsten Wind Tunnel. The drag

coefficients for the balls in the different tunnels differ due to the different designs of the tunnels producing different interferences. However the profile of these flows can still be compared.

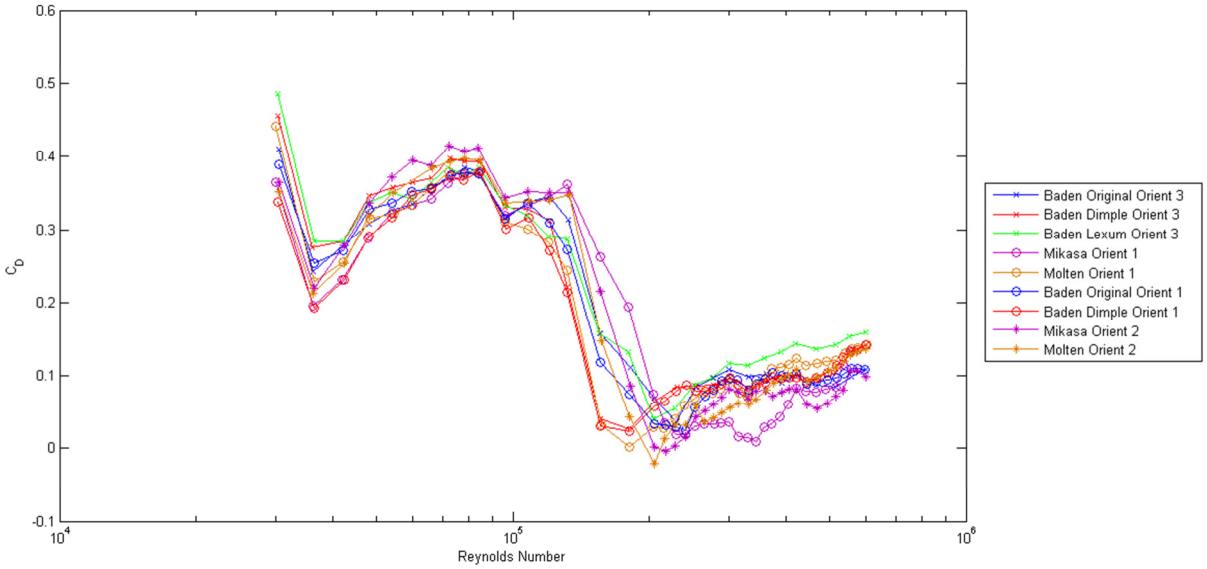

Figure 5: Kirsten Tunnel Drag Performance

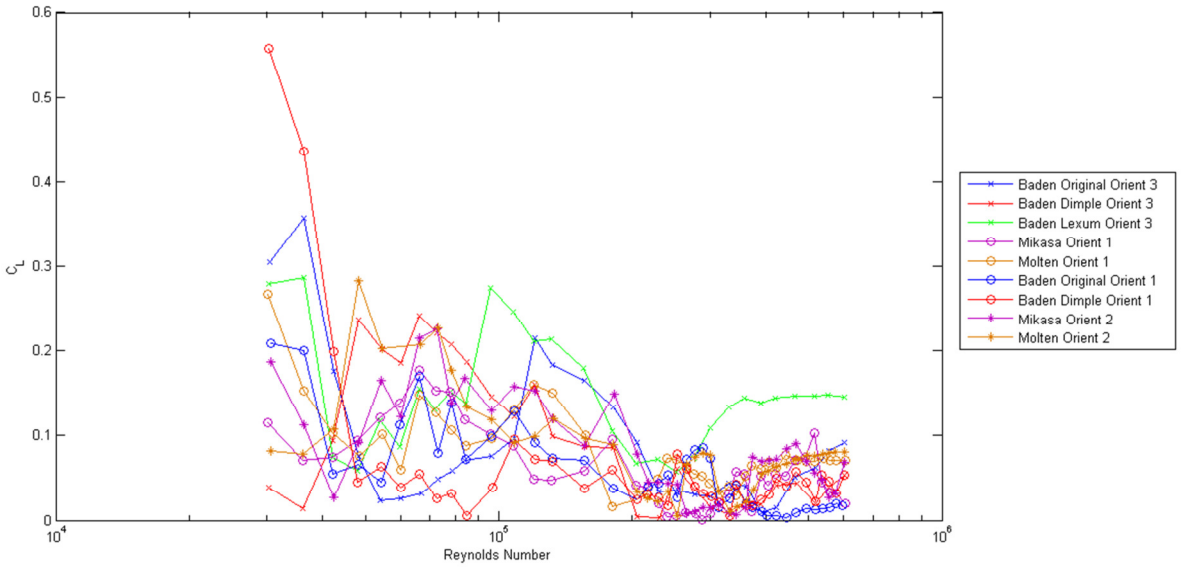

Figure 6: Kirsten Tunnel Lift Performance

Figure 5 shows that the Dimple ball experiences its drag crisis at about a Re of 1.56 x 10^5, while the Original and Lexum balls experience theirs closer to a Re of 2.0 x 10^5. The drag crisis occurs in spheres when the flow is turbulent enough that after laminar boundary layer separation, the boundary layer is able to reattach as a turbulent boundary layer. By reattaching as a turbulent boundary layer, flow

separation is postponed. Laminar boundary layers on spheres separate around 85 degrees from the stagnation point. This point can be described by drawing a straight line that parallels the flow and intersects the center of the sphere. Where the line also intersects the upwind surface of the sphere is the stagnation point. When the sphere goes beyond the critical Reynolds number and develops a turbulent boundary layer, boundary layer separation occurs around 120 degrees from the stagnation point (Achenbach, 1972). This delayed separation reduces the wake behind the sphere and lowers the pressure drag.

If a sphere is roughened through either the texture of the surface or by adding cavities to trip the boundary layer, the drag crisis can occur at a lower Reynolds number. Figure 7 illustrates how the drag crisis can shift for a ball when it is roughened. It also shows that as the Reynolds number gets bigger, a smoother ball will produce less drag than a rough ball once it has passed its drag crisis. This is because the rough ball produces more skin friction. The dimples in the Baden Dimple ball had the effect of shifting the ball's drag crisis to a lower Reynolds number (compared to the Baden Original or Lexum) which is beneficial because it means that it will experience the benefits of lower drag production at low speeds. The Baden Lexum's rougher surface did not shift its drag crisis significantly (compared to the Baden Original) but it did produce more skin friction for the ball. As the Reynolds number increases, the Kirsten drag data supports the findings from the Low Speed Wind Tunnel: from a Re of 2.5×10^5 to a Re of 5.0×10^5, the Lexum ball produces the most amount of drag while the Original ball in general produces the least.

The lift data in Figure 6 shows that at low Reynolds number, the amount of lift produced by the Original ball and the Dimple ball can vary greatly based on the configuration in flight. However, as the Reynolds number passes a Re of 2.5×10^5, the variations decrease and the lift values become steadier for these balls. The Lexum ball produces the highest lift above a Re of 2.5×10^5, just like the results found from the Low Speed Wind Tunnel. Unfortunately there was not enough time to run more configurations of the Lexum ball in the Kirsten Wind Tunnel.

Figure 7: Drag Crisis for a Sphere (Stanford University, 2007)

3.2 Comparing New Models

Other models of volleyballs were also tested to see how their designs influenced their performance characteristics. The models chosen were the Mikasa MVA200 and the Molten V5M5000 as shown in Figure 8. The seam characteristics for these balls are listed in Table 1while the dimple dimensions are listed in Table 2 (the Molten ball has raised hexagons rather than dimple cavities so the dimensions of a leg of the hexagon is listed). Both of these balls are made of composite material, though not necessarily the same composite material as the Baden Lexum and Dimple balls, as the Mikasa ball is noticeably smoother than the Lexum ball. The Mikasa and Molten ball also differ significantly from the Baden balls in that their seam depths are less than that of the Baden balls.

Figure 8: Mikasa and Molten Volleyballs. A front profile of the Mikasa ball in configuration 1 (a) and the Molten ball in configuration 1 (b).

Table 2: Dimple Dimensions

Make	Model	Depth (in)	Width (in)	Aspect Ratio (width/depth)	Surface Area (in^2)
Baden	VX450-02	0.008	0.104	13.83	39.71
Mikasa	MVA200	0.005	0.059	11.83	20.73
Molten	V5M5000	0.005	0.034	6.70	21.95

The Mikasa and Molten balls have completely different panel designs from the Baden balls. This means that the area covered by the seams on the ball is different. The Mikasa ball with its eight panels has a total seam length of only 98.98 inches, which is about one third less of the total seam length of the Baden balls (153.78 inches). The seam surface area referenced in Table 1 is obtained by multiplying this seam length by the width of the seams (for some perspective, the total surface area of a volleyball is approximately 214.91 in^2.) The different panel designs also mean that comparing balls by each configuration or orientation would not be advantageous. Instead the balls were compared based on the mean of all orientations. The drag and lift performance for all nine orientations of each model were averaged at different Reynolds numbers. The mean and standard deviations of these sets of nine orientations were plotted to show the average performance and the volatility of the models about the mean. The plot for drag characteristics can be found in Figure 9 and the plot of lift characteristics is in Figure 10.

The figures below show that the least drag and lift producing volleyball in the range of 44-100 fps is the Mikasa and the highest drag and lift producing volleyball is the Baden Lexum. The Molten ball outperformed the Baden Original and Dimple in the lift category, but did not do better than the Baden Original in the drag category. Again it is noted that the coefficient lift data, both mean and standard deviation, remain fairly constant as flow speeds increased. The mean coefficient of drag data on the other hand increases as the Reynolds number increase and the standard deviation data tends to decrease as speed increases (with the exception of the Mikasa standard deviation.)

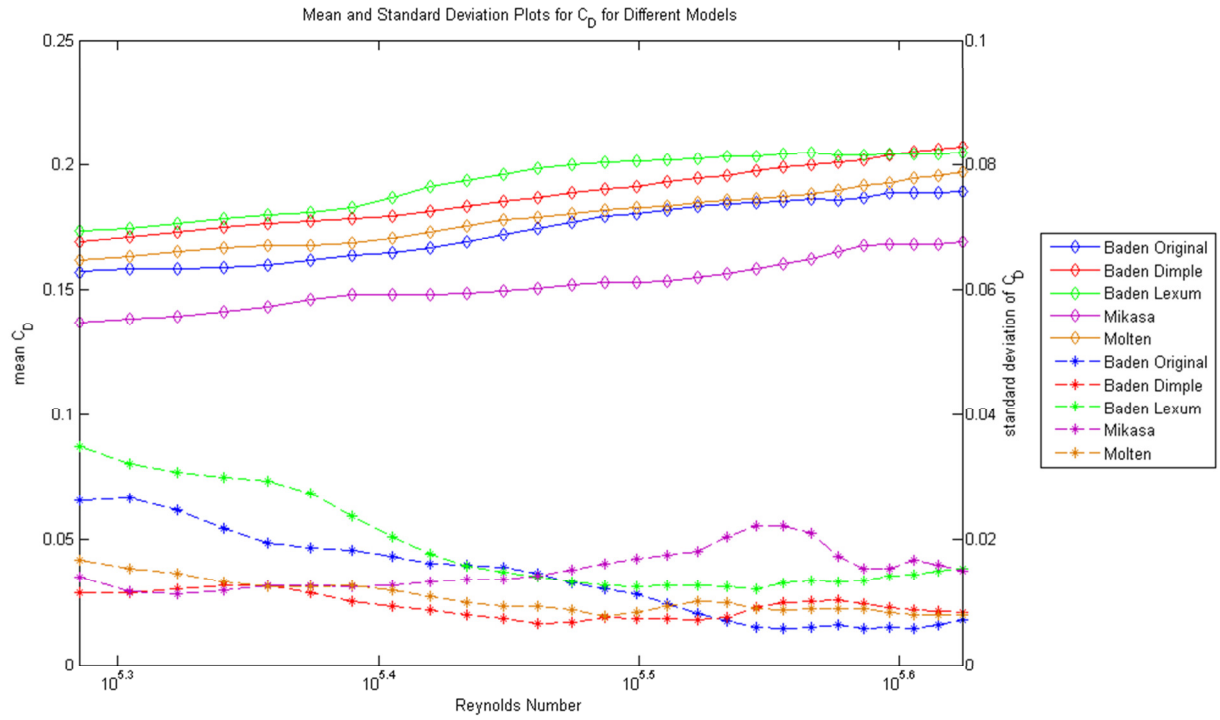

Figure 9: Drag Performance for All Models. Mean values are indicated by diamonds and standard deviations are indicated by asterisks.

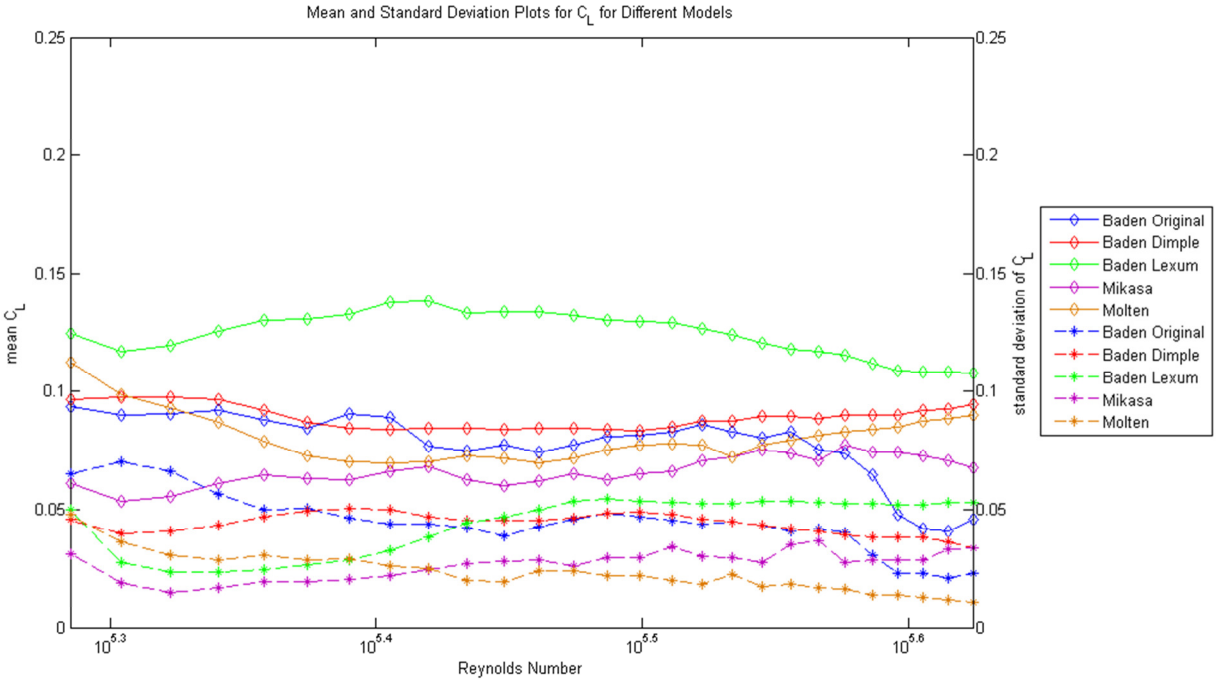

Figure 10: Lift Performance for All Models. Mean values are indicated by diamonds and standard deviations are indicated by asterisks.

Looking back at the Kirsten data it can be seen that while the critical Reynolds numbers for the Molten ball did shift towards a lower Re when compared to the Baden Original (which is the more traditional design of a volleyball), it did not shift as much as the Baden Dimple (Figure 5). And the Mikasa ball did not shift from the Baden Original drag crisis at all. So at lower speeds than those measured in Figure 9, the drag characteristics of the Baden Dimple ball perform the best.

3.3 Adjusting Skiving

Many modern, indoor volleyballs no longer have a cover sewn over the internal bladder so a seam is not necessary for constructing the volleyballs. However panels are required by regulation, so the edges of the panels are skived (shaved down) and epoxied onto the bladder, producing a faux seam. Baden Sports, Inc. was able to provide additional samples of their Original ball that had modified seams. One had minimal skiving applied; the other had no skiving applied at all (a depth and width was still measured for the seams of ball that had no skiving because the panels did not match up perfectly). By having volleyballs with the same design but different seam dimension, the seam dimensions could be isolated as a variable and their effect on performance could be studied. Photos of their differences can be seen in Appendix E and their seam dimensions are listed in Table 1.

Reducing skiving of the ball improved the drag performance of the ball. As can be seen in Figure 11, reducing the skiving reduces the coefficient of drag of the ball, especially at the lower Reynolds numbers. In the case of the Minimum Skiving ball, it produces lower coefficients of drag than the Mikasa ball, the best drag performing ball of current models. However, it diminished the lift performance of the ball (Figure 12) by producing more lift at low Reynolds numbers than even the Baden Lexum ball. Of note, the mean of the coefficients of lift change as the speed changes for the Minimum Skiving ball and No Skiving ball which is different from every other model's lift performance at this speed range. By looking back at Figure 5 and Figure 6 it can be seen that the coefficient of lift for each of models stabilizes at a low point below 0.1 after each model has passed through its critical Reynolds number. It appears that while the coefficient of drag is descending to the critical Reynolds number, the coefficient of lift is unstable. It is not until after the coefficient of drag has begun increasing again with increasing Reynolds number that the coefficient of lift stabilizes. This would imply that the Minimum Skiving and No Skiving balls in the Low Speed Tunnel tests are measured just after the balls have passed through the drag crisis but before their lift profiles can stabilize. Their seam characteristics make them closer to a pure sphere than any other ball which means they likely pass through drag crisis at a higher Reynolds

number value than the other models. Unfortunately the Baden Minimum Skiving and No Skiving balls were not able to be tested in the Kirsten Wind Tunnel to verify this theory.

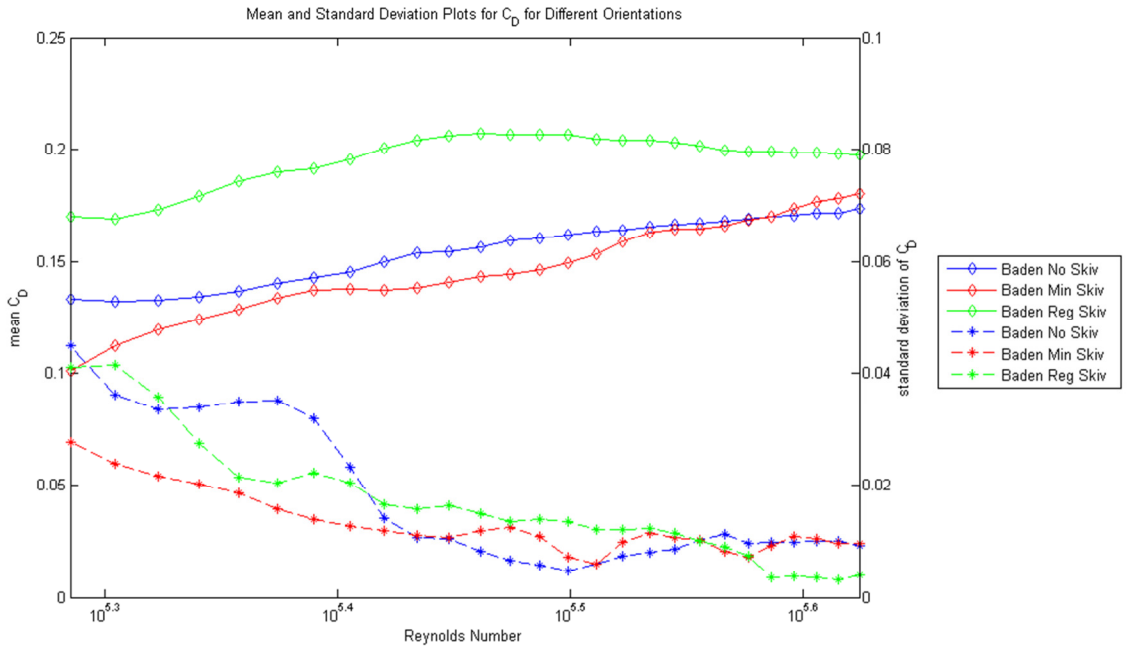

Figure 11: Drag Performance with Changing Skiving. Mean values are indicated by diamonds and standard deviations are indicated by asterisks.

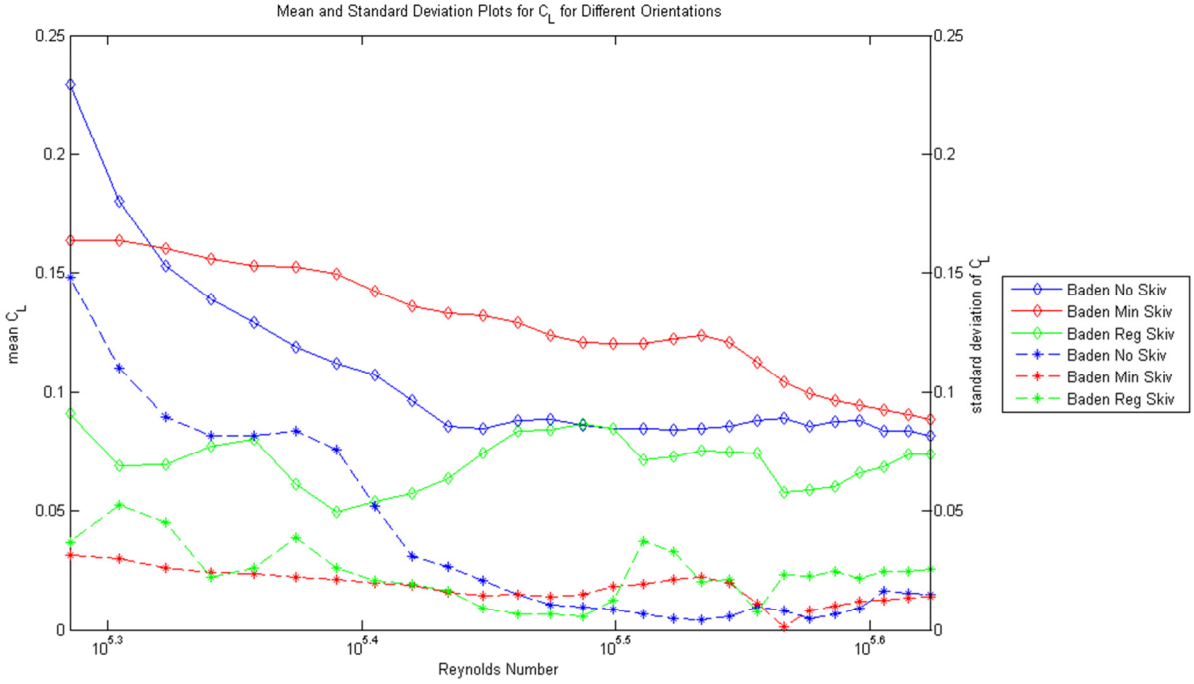

Figure 12: Lift Performance with Changing Skiving. Mean values are indicated by diamonds and standard deviations are indicated by asterisks.

3.4 Cavity Flows and Momentum Thickness

The volleyball can be viewed as an extremely complex cavity flow problem. It is complex because it is a sphere so the flow across the surface is not uniform, it has multiple cavities in different locations, and the seams that form the cavities are at different angles and orientations. The Graduate Aerospace Laboratories at the California Institute of Technology is looking at how adding a single bump can affect the lift and drag performance of a sphere (Oliwenstein, 2011). In the situation of a volleyball, it is difficult to view each cavity or abnormality individually because it is impossible given the setup to calculate what amount of lift and drag was caused by each individual cavity. For that reason the cavities were viewed as a set of cavities. A cavity's effect on the ball would be based on how significant the cavity was (quality) and how often the cavity appeared on the surface of the ball (quantity). The quantity factor was determined by dividing the surface area of the cavity or dimple by the total surface area of a volleyball (214.91 in^2). This factor can be found in Table 3 and accounts for the width and length of the seams/dimples and allows all balls to be compared regardless of how populated with seams and dimples they may be. The quality factor is determined by relating the last dimension of the seams, depth, to the momentum thickness. The momentum thickness is the length that equates to the amount of momentum lost in the flow due to the presence of the boundary layer (Kundu & Cohen, 2008). This is useful because the size of the momentum thickness can determine to what degree the cavity affects the flow around the ball. If the momentum thickness is significantly larger than the depth of the cavity, than the cavity does not affect any flow outside of the boundary layer and does not reduce the free flow stream. The momentum thickness for this research was determined using standard day conditions and was approximated with the Blasius solution shown in equation (17).

$$\boldsymbol{\theta^* = 0.664D/\sqrt{Re}} \qquad \textbf{(17)}$$

This is only an approximation because the Blasius solution applies to laminar flows and the ball experiences both laminar and turbulent flow as the air passes over it. However, this number provides a reference to compare the seam dimensions to and it creates a means to non-dimensionalize the seam dimensions. The momentum thicknesses for four different speeds tested are listed in Table 4. These numbers provide a basis for comparing the depths of the cavities. By dividing the cavity depth by the momentum thickness at these different velocities, we can compare how the quality of the cavities affects the performance of a ball. These depth quality factors for four different speeds are listed in Table 3.

Table 3: Ball Quantity and Depth Quality Factors

Make	Model	Quantity Factor	Quality Factor			
			44 fps	62 fps	80 fps	98 fps
Baden	VX5E-01	20.1%	2.18	2.59	2.94	3.26
Baden	VX450C-230	20.8%	2.30	2.74	3.11	3.44
Baden	VX450-02	21.3%	2.18	2.58	2.94	3.25
Mikasa	MVA200	13.9%	1.65	1.96	2.23	2.46
Molten	V5M5000	17.3%	1.61	1.92	2.18	2.41
Baden	VX5E-01 (Min Skiv)	12.2%	2.15	2.55	2.90	3.21
Baden	VX5E-01 (No Skiv)	9.7%	0.54	0.65	0.73	0.81

Table 4: Momentum Thickness at Various Speeds

Speed (fps)	Reynolds Number	Momentum Thickness
44	1.93×10^5	0.0125
62	2.72×10^5	0.0105
80	3.51×10^5	0.0093
98	4.30×10^5	0.0084

What is evident from these tables is that the Baden No Skiv ball is far below the other balls in terms of the quantity and depth quality factors of its seam cavities. The Mikasa and Molten balls are also lower than the non-altered Baden balls in terms of their quantity and depth quality factors. To bring both quality and quantity together to judge performance against one dependent variable, a cavity factor z is derived by multiplying the depth quality factors by the quantity factors as shown in equation (18).

$$z = \frac{d_{seam}}{\theta^*} \frac{SA_{seam}}{SA_{total}} \quad (18)$$

This cavity factor z does not include the effects of the dimples because the dimple depths were smaller than the momentum thickness so they would not have a significant effect on the drag. This is evident in the fact that the only major difference between the Baden Lexum ball and the Baden Dimple ball is the dimples and their drag profiles from Figure 9 are very similar. Plotting the coefficients of drag versus z for the different models in Figure 13 shows some trends. The slope of the plots for the Baden No Skiv ball and Baden Min Skiv ball were much steeper than those of the other balls. This likely goes back to the fact that the Reynolds numbers for these balls are still close to the drag crisis for these balls.

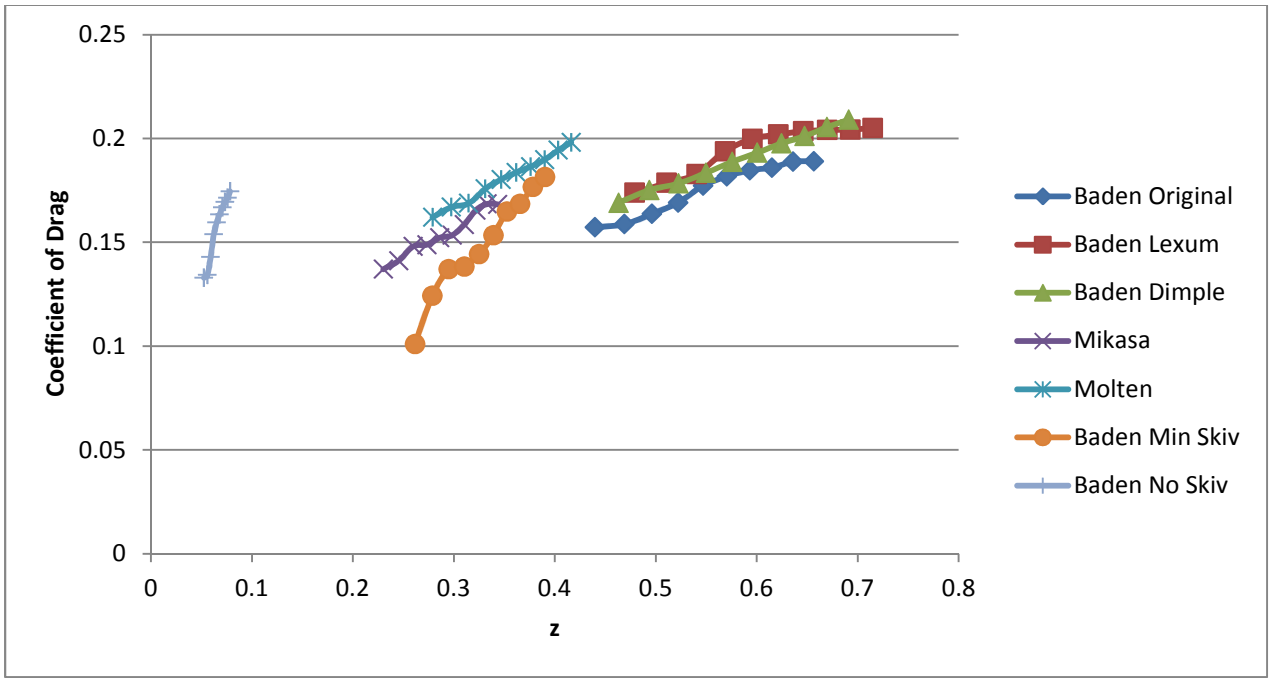

Figure 13: Drag Performance Related to z

The sharp contrast in the profile of the Baden Minimal Skiving and No Skiving balls from the other models could also be related to the seam width to momentum thickness ratio. Gharib and Roshko found that as the cavity width to momentum thickness ratio is increased beyond certain key values, the flow enters different modes of oscillation which would affect the drag experienced by the ball in the flow (Gharib & Roshko, 1987). Looking at Table 5, it can be seen that the Minimal Skiving and No Skiving balls have a seam width to momentum thickness ratio that is almost 40% less than that of the other balls. It could be that the seams of these balls are operating in a different mode and that is why their profiles are so different.

Table 5: Ball Seam Width Quality Factors

Make	Model	Width to Momentum Thickness Ratio			
		44 fps	62 fps	80 fps	98 fps
Baden	VX5E-01	22.52	26.73	31.48	33.60
Baden	VX450C-230	23.23	27.58	32.48	34.67
Baden	VX450-02	23.77	28.22	32.05	35.48
Mikasa	MVA200	24.22	28.75	32.66	36.14
Molten	V5M5000	18.37	21.82	24.79	27.44
Baden	VX5E-01 (Min Skiv)	13.59	16.14	18.33	20.29
Baden	VX5E-01 (No Skiv)	10.79	12.80	14.54	16.10

The other balls had linear trends that all seemed to intercept around 0.845. Excluding the Baden Min Skiv and Baden No Skiv, there appears to be a correlation between the depth of the seams and the slopes exhibited in Figure 13. Non-dimensionalizing the depths by the ball diameter (this was so that a constant length scale would be used rather than momentum thickness which changes with speed), a function h was found for the slope of the lines such that:

$$h = -89.569\frac{d}{D} + 0.4767 \quad (19)$$

This slope factor h was multiplied by the cavity factor z and plotted on Figure 14. Other than Baden Min Skiv and Baden No Skiv, these factors correlate exactly with the coefficient of drag producing a 1:1 ratio. The lines do not match up entirely which could be due to the remaining differences in the balls that can't be accounted for here such as the seam pattern, the dimple pattern or hexagon pattern, and the roughness of the balls. Roughness likely plays a large role in this as the roughest ball surfaces (as seen in Appendix C) were on the Baden Lexum and Molten balls while the smoothest surfaces were on the Mikasa and Baden Original balls. A 1:1 correlation line is drawn on Figure 14 showing that the Baden Lexum and Molten balls remain just above the correlation line while the Baden Original and Mikasa balls lie just below it. This shows that surface roughness increases the amount of drag a volleyball will produce. It is also possible to interpret Figure 13 as showing that a logarithmic relationship exists between the coefficient of drag and the factor z. However this theory is difficult to support without more data points to show a clear curve.

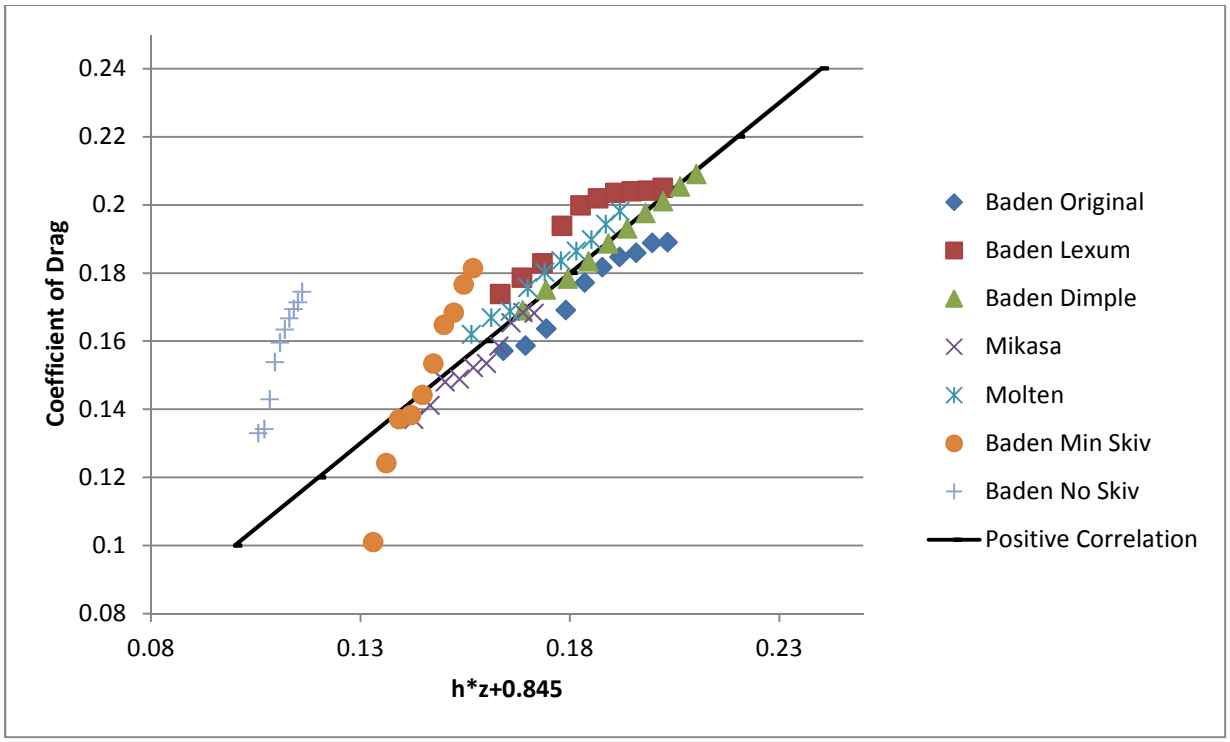

Figure 14: Correlation Between Drag and z

A relationship between the influence of the cavities and the lift performance of the balls was not as clear. Plotting the coefficient of lift against the cavity factor did not show any clear patterns. So the coefficient of lift was plotted against a second cavity factor, y, which consists of the cavity width to momentum thickness ratio multiplied by the cavity surface area to ball surface area ratio as shown in equation (20). Here the dimple characteristics are taken into consideration and the quantity and width quality factors are listed in Table 6.

$$y = \frac{b_{seam}}{\theta^*}\frac{SA_{seam}}{SA_{total}} + \frac{b_{dimple}}{\theta^*}\frac{SA_{dimple}}{SA_{total}} \quad (20)$$

Table 6: Ball Dimple Quantity and Width Quality Factors

Make	Model	Quantity Factor	Quality Factor			
			44 fps	62 fps	80 fps	98 fps
Baden	VX450-02	0.101%	8.29	9.85	11.18	12.38
Mikasa	MVA200	0.035%	4.73	5.61	6.37	7.06
Molten	V5M5000	0.037%	2.68	3.18	3.61	4.00

Figure 15 shows a plot of the lift coefficient related to the cavity factor, y. While drag increased as z was increased, lift decreases as y is increased. The coefficient of lift appears to be a logarithmic function of the inverse of y with the models approaching a lift coefficient of approximately 0.1 as y increases beyond 4. Similar to Figure 14, the rougher balls (Baden Lexum and Molten) are producing more lift than the smoother balls (Baden Original and Mikasa).

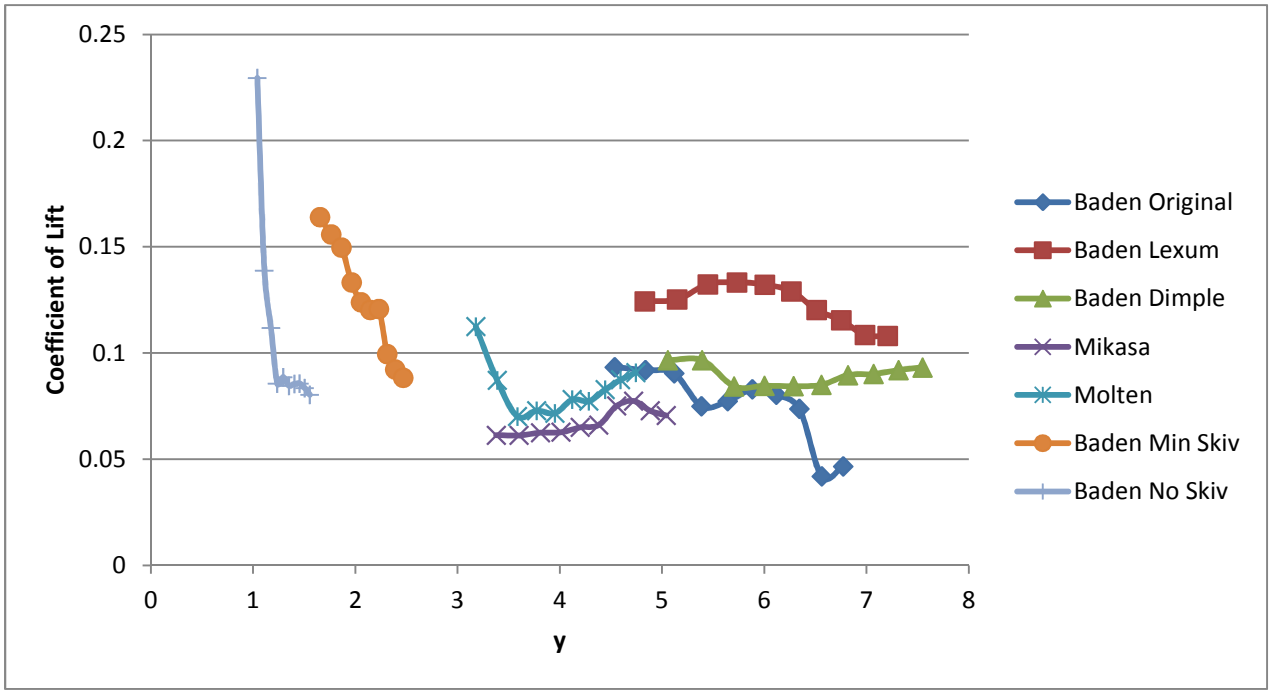

Figure 15: Lift Performance Related to y

CHAPTER 4: CONCLUSION

4.1 Discussion Analysis

A smooth sphere experiences its drag crisis at a Reynolds number of approximately 3.7×10^5 (Achenbach, 1972). This equates to about 80 fps, which is higher than most float serves are hit. For this reason the volleyballs need some degree of roughness to trip the boundary layer into a lower drag profile. Historically seams have been effective lowering the critical Reynolds number to 2.0×10^5; however the Baden Dimple has shown that additional cavities can be used to trip the boundary layer at a lower Reynolds number than balls with just seams alone. If there is less drag to overcome, this means that the players will exert less energy to hit the ball at those speeds. There is also appears to be positive correlation between the Reynolds number at which the lift coefficient stabilizes and the Reynolds number at which the drag crisis occurs. If a ball can be modified so that it's drag crisis occurs at a lower Reynolds number, than the lift coefficient of that ball should stabilize to its minimum at a lower Reynolds number as well.

The Baden Minimum Skiving and No Skiving balls produced different trends for lift and drag than the other balls. This is believed to be because their seam dimensions are so small that they approach the design of a smooth ball and therefore have a drag crisis that occurs at a higher Reynolds number than the other models. Figure 7 shows that the slope of the drag profile of a rough ball immediately after the drag crisis is very steep but as the Reynolds number increases, the slope becomes shallower. The Minimum Skiving and No Skiving balls are likely in the steep region while the other balls are in the shallow region. Their more rapidly changing drag adds to their instability and causes their lift production to be higher as well.

The drag coefficients for the other models were observed to increase linearly with the increase of z. The differences in the drag produced by the models studied were attributed to the skin friction of the balls and the depth of the seams. The deeper seams allow more of the airflow to dip into the seam and impact the trailing edge of the cavity, increasing the drag. However at Reynolds number values tested, the roughness of the ball (which determined the amount of skin friction produced) had as great if not a greater influence on the amount of drag produced as the seam depth.

The lift coefficients however decreased as y increased. Roughness was still a factor, but wider cavities on the ball produced a more stable lift profile. The Baden Dimple ball had the widest cavities and went through the drag crisis at a lower Reynolds number than the other balls supporting the theory that lift stabilizes after the ball has passed through the drag crisis. Based on the lift performance of the Baden

Minimum Skiving and No Skiving balls, it is likely that this lift stabilization takes place after the ball has gone through the steep portion in Figure 7 that comes just after the drag crisis and has moved into the shallow portion.

In the range of speeds from 44 fps to 100 fps, the Mikasa MVA200 is the best performing ball. It displayed the lowest drag profile as well as the lowest total lift profile. The characteristics that are attributed to causing its low drag profile are it's smooth surface (less skin friction) and its small seam depth. It's low lift profile is attributed to it's smooth surface, its large seam width, and its numerous dimples that created a uniform cavity surface to the ball.

4.2 Recommendations for Future Designs

The following are suggestions for parameters to use when designing future volleyballs.

1. Use leather or a similarly smooth material for the surface of the ball. While roughness was not the driving factor for performance, it did have an effect. Having a rough surface provides little benefit to the game (there is no need to ever grip the ball while the ball is in play) and it clearly increases the lift and drag produced by the ball.
2. To reduce the amount of drag produced, the first cavity factor, z, should be kept low. Drag increases linearly with z, however the linear relationship does not apply at low values of z. Values of z below 0.23 do not produce lower drag coefficients than those just above 0.23.
3. To reduce the amount of lift produced, the second cavity factor, y, should be kept above 4. The larger value stabilizes the lift generation of the ball near its minimum. The factor y can be increased by increasing the width of the cavities or increasing the surface area of the cavities. Both methods cause the volleyball to appear more uniform in flight regardless of orientation.

4.3 Improvements for Future Work

The number one improvement that could be made to future research in this field is to take more runs. With 18 different configurations of balls to gather data on, barring any errors in testing, only one run could be made for every orientation change of the configuration (three runs total for every configuration.). For each run, 10 second time averages were taken at each data point, so much of the randomness and noise were removed from the data. However more data always improves the accuracy of analysis. More configurations of the models would also have improved the quality of the results so that the mean and standard deviations would have been more accurate. Increasing the number of orientation changes would have helped as well. This could be accomplished with a new mount that went beyond +/- 5 degrees or by having more runs at angle changes below 5 degrees.

Another improvement to the technique of the data collection would have been to alter the step size. Changing the dynamic pressure by 0.5 pounds per square foot made sense at high values of dynamic pressure. However since velocity changes with the square root of dynamic pressure, changes of 0.5 pounds per square foot at lower values of dynamic pressure amount to large changes in the velocity of the airflow. At low velocities, a smaller step size would have produced smoother plots and provided a better understanding of where dramatic changes to properties occur.

The seam size was measured with analog calipers which allowed for a high degree of human error. Since the seams are curved and not sharp edges, the determination of the width and depth of the seam using calipers allows for some subjectivity. A better measurement technique would be to take a mold of the ball at the seam and use a more precise measurement device such as a laser displacement sensor or a coordinate measuring machine.

Since multiple seams and dimples were looked at in this experiment, future experiments should look at isolating the gap spacing between the seams/dimples. This research focused on the width of the seams/dimples, but with multiple cavities affecting the flow, the gap between the cavities should also be taken into consideration. Separation between cavities should be altered to see what impact that has on the performance of the balls. Along with isolating the gaps, the size of the dimples should be isolated as well. By maintaining the same amount of surface area for the dimples and altering the dimple widths, the effect of small versus large dimples can be measured.

Obtaining data at lower airspeeds would have made the data more applicable to the real world. A men's float serve is hit at initial speed of 44.5-54 feet per second. However women's serves are slower, coming in around 30-40 feet per second. This equates to a Reynolds number of 130,000-180,000, bringing them into the range of the drag crisis and out of the range of the Low Speed Wind Tunnel. To obtain a better understanding of the flow at these key velocities, another wind tunnel that can accurately record data at those speeds (such as the Kirsten Wind Tunnel) should be used. Lowering the speed would also allow data to be gathered on both sides of the drag crisis, which would provide a better understanding of how different ball designs go through the drag crisis.

Frequency data for the volleyballs in the Low Speed Wind Tunnel was not obtained but could be useful for future research. These experiments looked at time-averaged data which disregards oscillations; however those oscillations could improve the understanding of how the flow is interacting with the cavities. Frequency data would provide information on how ball designs affect the frequency, mode, and amplitude of the oscillations of the volleyballs.

Finally, the parameter that this experiment referenced but did not study in depth is roughness. It is difficult to quantify but should not be discounted. Roughness in models was compared subjectively in this experiment, but better instrumentation could provide a more qualitative comparison of the roughness of the different balls and create a more accurate understanding of the effects of roughness.

BIBLIOGRAPHY

Achenbach, E. (1972). Experiments on the flow past spheres at very high Reynolds numbers. *Journal of Fluid Mechanics, 54*, 565-575.

Asai, T., Ito, S., Seo, K., & Hitotsubashi, A. (2010). Aerodynamics of a New Volleyball. *Procedia Engineering 2*, 2493-2498.

Gharib, M., & Roshko, A. (1987). The effect of flow oscillations on cavity drag. *Journal of Fluid Mechanics, 177*, 501-530.

Hayrinen, M., Lahtinen, P., Mikkola, T., Honkanen, P., Paananen, A., & Blomqvist, M. (2007). Serve Speed Analysis in Men's Volleyball. *Science for Success II.* Jyvaskyla, Finland: KIHU-Research Institute for Olympic Sports.

Kundu, P. K., & Cohen, I. M. (2008). *Fluid Mechanics* (4th ed.). Burlington, MA, USA: Academic Press.

Mikasa Sports. (2008, June 27). *Mikasa Sports News.* Retrieved January 12, 2012, from Mikasa Sports USA: http://mikasasports.com/new-volleyball-debuts-at-the-2008-beijing-olympic-games.html

Molten Corporation. (n.d.). *Volleyball, Molten Sports Division*. Retrieved November 22, 2011, from Molten Sports Division (Molten Corporation: http://www.molten.co.jp/sports/en/volleyball/index.html

Oliwenstein, L. (2011, Winter). Roughing It. *Engineering & Science, LXXIV*(1), pp. 16-21.

Pankhurst, R. C., & Holder, D. W. (1965). *Wind-tunnel technique: An account of experimental methods in low and high-speed wind tunnels.* London: Pitman.

Stanford University (Ed.). (2007). Multimedia Fluid Mechanics. (2nd). Palo Alto, CA, USA: Cambridge University Press.

Thorsteinsson, H. (n.d.). *FIVB Volleyball Homologation Procedure.* Retrieved February 20, 2012, from Federation Internationale De Volleyball Homepage: http://www.fivb.org/en/Technical/Homologation/FIVB_Volleyball_Homologation_Procedures.pdf

Wei, Q.-d., Lin, R.-s., & Liu, Z.-j. (1988). Vortex-induced dynamic loads on a non-spinning volleyball. *Fluid Dynamics Research 3*, 231-237.

Wilcox, D. C. (2010). *Basic Fluid Mechanics.* La Canada: DCW Industries, Inc.

APPENDIX A : LABVIEW

The visual code for the Labview program used to gather the data from the Low Speed Wind Tunnel can be found at the following site:

https://sites.google.com/a/aa.washington.edu/volleyball-aerodynamics/labview-code

APPENDIX B : MATLAB CODE

The MATLAB code used to interpret the wind tunnel data gathered can be found at the following site:

https://sites.google.com/a/aa.washington.edu/volleyball-aerodynamics/matlab-code

APPENDIX C : CONFIGURATION IMAGES

Photos of the different configurations of volleyballs tested during this experiment can be found at the following site:

https://sites.google.com/a/aa.washington.edu/volleyball-aerodynamics/photos/orientation-photos

APPENDIX D : TEXTURE IMAGES

Figure 16: Baden Original Texture

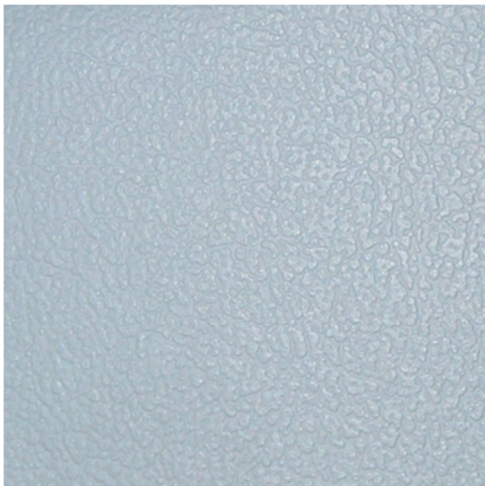

Figure 17: Baden Lexum Texture

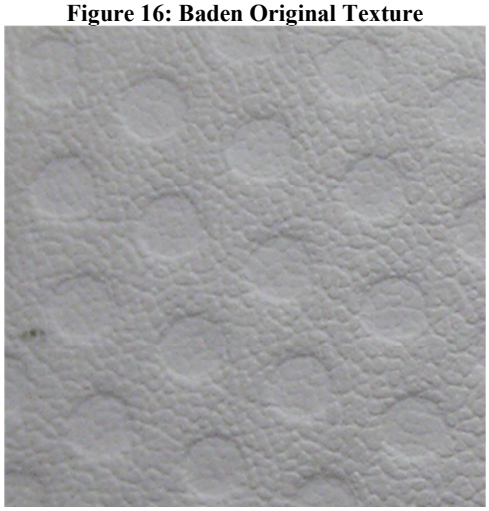

Figure 18: Baden Dimple Texture

Figure 19: Mikasa Texture

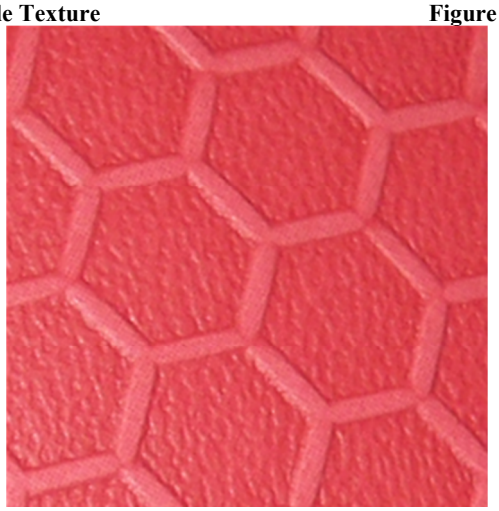

Figure 20: Molten Texture

APPENDIX E : SEAM IMAGES

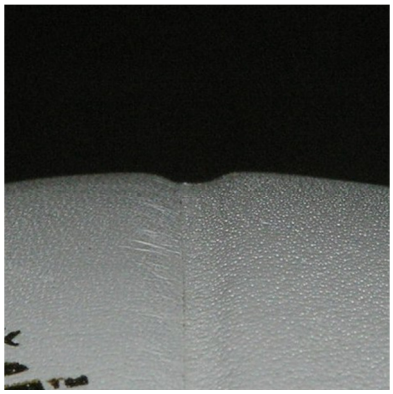

Figure 21: Baden Original Seam

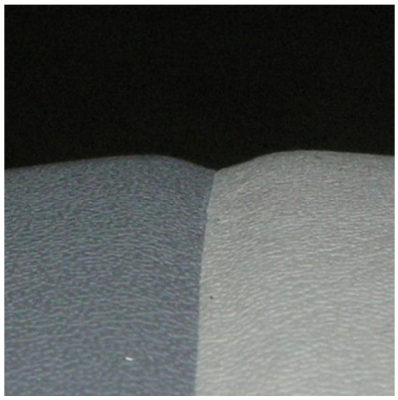

Figure 22: Baden Lexum Seam

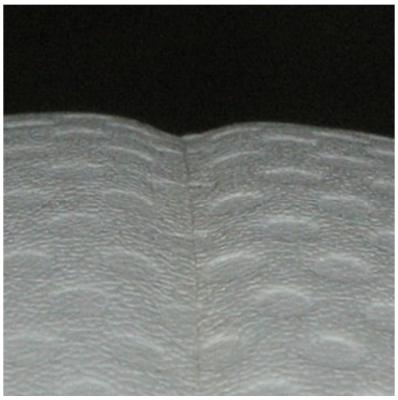

Figure 23: Baden Dimple Seam

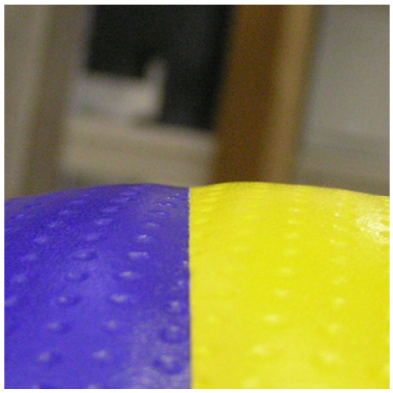

Figure 24: Mikasa Seam

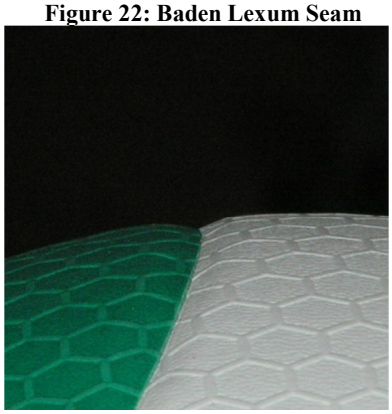

Figure 25: Molten Seam

Figure 26: Baden Min Skiv Seam

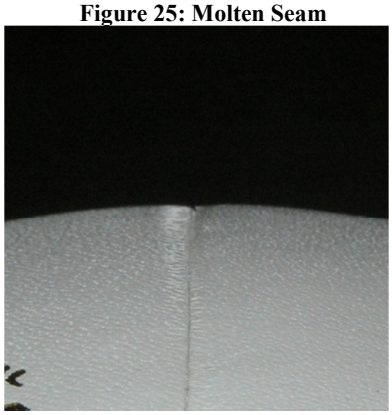

Figure 27: Baden No Skiv